BIRZEIT UNIVERSITY

Faculty of Science

Department of Physics

PHYS411—Seminar in Physics

Realizing quantum spin hall edge states in small open Honeycomb systems

Prepared by:

Khaled Hasan—1210265

Supervisor: Prof.Abdallah Sayyed Ahmad

Date: June 24, 2025

Abstract

Graphene-like quantum dots with a honeycomb lattice exhibit unique electronic properties due to quantum confinement and edge effects, promising for low-dimensional physics, spintronics and quantum computing. Although some interesting topological phases, such as quantum spin Hall (QSH) edge states, are theorized in systems such as graphene nanoribbons, it is unclear whether small confined honeycomb dots can support similar phases. Finding such topological phases in small open systems would be valuable in developing technological devices such as topological qubits. In this work, we explore the existence and characteristics of edge states in honeycomb open systems using a tight-binding model. We numerically investigate how external perturbations—such as magnetic fields, spin-orbit coupling (SOC), next-nearest-neighbor interactions, and edge potentials and impurities—influence these states and their robustness of edge states. Additionally we study the topology of the quantum dots using the Bott index (topological invariant in real space) extended to real space, and plotting quantized spin polarized conductance.

Our research confirmed that Triangular zigzag quantum dots and large honeycomb dots exhibit degenerate zero-energy edge states, while armchair-edged dots remain gapped and lack such states even at larger sizes; the quantum spin Hall effect can be realized in small open honeycomb systems with spin-orbit coupling, as demonstrated by a integer Bott index and quantized spin-polarized conductance, with edge states robust against disorder but suppressed by strong staggered potentials or large next-nearest-neighbor hopping, and the quantized conductance calculations revealed a enhancement mechanism by tuning the staggered potential against the real part of the next-nearest-neighbor hopping, and revealed an oscillating back scattering and coupling between the edge and bulk states due to finite size effects.

Contents

List of Figures

1 Introduction

Graphene is a monolayer two-dimensional material made of a hexagonal lattice of carbon atoms, the small effective mass of its electrons and the linear dispersion near some of its reciprocal lattice points "Dirac points" (therefore have a relativistic nature as we show in appendix A) makes it suitable for different technologies in spintronics, sensors, and other quantum devices. These unique properties drew the attention of researchers to investigate electronic, magnetic and optical properties of Graphene nanostructures[3][6].

Among the key electronic features of graphene nanostructures is the realization of zero or quazi-zero energy eigenstates, that are localized on the sample edges. These states allow for a special electronic transport mechanism through the sample edges. In honeycomb lattices like graphene, the existence and nature of edge states depend strongly on the type of edge termination. These types are **armchair edges**, which consists of the two sublattices. And **zigzag edges**, where the edge has one sublattice type. It was shown that honeycomb structures with armchair edges do not host edge states and are gaped around the fermi-energy, while zigzag edges, in general, have quazi-zero edge states[3][1].

While generic terminated boundaries of Honeycomb nanostructures are "zigzag-like" and can be used to realize edge states (as discussed in section2.2)[1]. Yet for most geometries, these edges are localized within a portion of the edge, that is, they cannot be used for electron transport. An especially compelling phenomenon associated with edge states is the quantum spin hall effect, or the two-dimensional topological insulators. Where the edge hosts a Kramer pair of degenerate spin polarized edge states with opposite spin and opposite Chiral propagation at edges, while the bulk remain insulating (gaped). Due to the bulk gap, these edge states are robust and protected against perturbations and disorders, unless the bulk gap is closed. When the bulk gap closes, the system undergo what is called a **topological transition**. This relationship between the edge states and the gaped bulk is called bulk edge correspondence. This specific property is prominent in the applications in quantum computing and quantum error corrections[4].

In the QSH topological phase, the bulk energy gap opens due to spin-orbit coupling, preserving time-reversal symmetry (thus protected by it). Therefore, while typically time-reversal symmetry will prevent currents from flowing. A spin polarized current can flow along the edges. While Kane and Mele hypothesized that the graphene nanoribbons can host quantum spin hall states[11], observing this experimentally is exceptionally challenging, since graphene has extremely low spin orbit coupling coefficient. With that being said, some numerical simulations have suggested adding adatoms to graphene lattice in order to enhance SOC[18], however, aside from increasing the SOC coefficient, it will also increase the nnn-hopping which negatively affects the stability of the observed QSH effect as we will demonstrate in this paper.

While we begin by investigating graphene, we will not be concerned with the specific details of graphene, but rather we will focus on the general properties of honeycomb lattices and their edge states.

In this work, we numerically investigate edges of honeycomb nanostructures. Confirming that graphene triangular zigzag quantum dots (TZQD), zigzag graphene nanoribbons, and large Graphene dots have delocalized degenerate edge states with Fermi energy[7, 20]. These states are metallic in nature, since they intersect the Fermi energy, thus relevant for technological applications. We then proceed by studying the robustness and topology of these edge states, we used the Bott index to indetify the phase transition between the topological phase and the trivial phase. We finally study the conductance quantization using the Landauer-Büttiker formula.

2 Identifying edge states

In this section we will consider honeycomb quantum dots and prove the existence of localized edge states, we will do that by solving the tight binding model equations for the zero energy states (in the unperturbed case). We begin by simple TB model with NN-hoppings, thus preserving time reversal symmetry, (which is a good approximation for cases like graphene[18]).

2.1 Nanoribbons

We begin by considering the tight binding model for a graphene nanoribbons that extend infinitely in the x-direction (index m) and terminates in the y-direction (index $n \in \{1, 2, \ldots, N\}$) is given by

$$H = -t \sum_{n,m} \left(a_{n,m}^\dagger b_{n,m} + a_{n,m}^\dagger b_{n-1,m} + a_{n,m}^\dagger b_{n,m+1} + h.c \right) + \sum_{\langle\langle i,j \rangle\rangle} \left(t_{ij}' a_i^\dagger b_j + h.c \right) \quad (1)$$

Using Fourier transformation in the x-direction in terms of the sublattice's creation and annihilation operators $a_{n,m}(b_{n,m}) = \sum_k a_{n,k}(b_{n,k})e^{ik\,ma}$ we get

$$H(k) = -t \sum_n \left[\left(1 + e^{-ika}\right) a_{n,k}^\dagger b_{n,k} + a_{n,k}^\dagger b_{n-1,k} + h.c \right] \quad (2)$$

Since the edge is a zigzag one consisting of one sublattice (say A without loss of generality), we can treat the edges associated B lattice point as an empty B site ($b_{1,k} = \hat{0}$), while the opposite is true for the other edge $a_{N,k} = 0$.

For the case of zero or quazi-zero energy eigenstates, we have

$$\varepsilon b_n = \left(1 + e^{ika}\right) a_n + a_{n+1}$$
$$\varepsilon a_n = \left(1 + e^{-ika}\right) b_n + b_{n-1}$$
$$a_{n+1} \approx -\left(1 + e^{ika}\right) a_n$$
$$b_{n-1} \approx -\left(1 + e^{-ika}\right) b_n$$
$$a_{n+1} \approx (-1)^n \left(1 + e^{ika}\right)^n a_1 = \left(-e^{ika/2}\right)^n (2\cos(ka/2))^n \quad (3)$$
$$b_1 \approx (-1)^n \left(1 + e^{-ika}\right)^n b_{n+1} = \left(-e^{-ika/2}\right)^n (2\cos(ka/2))^n \quad (4)$$

(a) $H(k = 2\pi/3 - 0.3)$

(b) $H(k = 2\pi/3 + 0.3)$

(c) The band structure of the nanoribbon, $k_x = \pm 2\pi/3$ are denoted by vertical red line
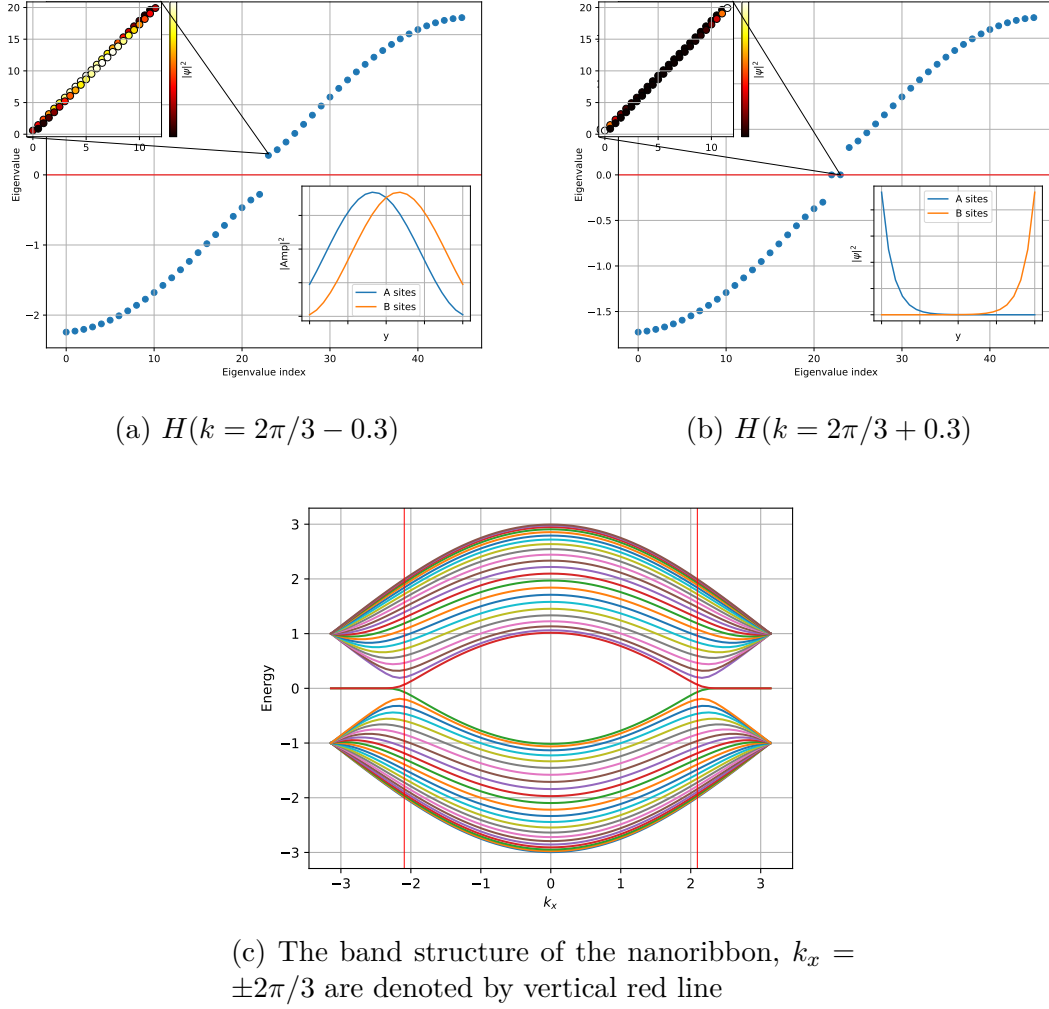
Figure 2.1: infinite naboribbon transition between phases that support and does not support edge states. The fermi energy is labeled by the red line.

In order to recover the boundary conditions $a_N = b_1 = 0$ from equation 3 it is clear that the intensities at sites a and b have to decay, in order to achieve that one has to have $|1 + e^{ika}| = |2\cos\frac{ka}{2}| < 1$, that is, $k > \frac{2\pi}{3a}$, otherwise, there will be no propagating edge states (see figure 2.1) It is therefore clear that infinite nanoribbons support propagating Fermi energy edge states under certain values of the momentum $|k_x| > \frac{2\pi}{3a}$, a similar argument was proved using a continuous model with Dirac formula can be found in [6] and [5].

2.2 General Terminated Lattice

Here we summarize the work done in [1] to study the properties of terminated honeycomb systems and their general boundary conditions both in analytical and numerical settings. This approach will be useful in dealing with realistically sized quantum dots (of the order of $\mathcal{O}(10 \text{ nm})$). The key physical requirement at a terminated boundary is the vanishing normal

current $\psi^\dagger(\hat{n} \cdot \vec{J})\psi = 0$, however this is not sufficient to uniquely determine a solutions. As an example, consider the ribbon discussed above, a nanoribbon extending in the $\hat{x}$ direction is $\psi^*_{A(K)}\psi_{B(K')} + \psi^*_{A(K')}\psi_{B(K)} = \psi_{A(K)}\psi^*_{B(K')} + \psi_{A(K')}\psi^*_{B(K)}$. In general it was shown that the general boundary conditions are of the form of $\psi = M\psi$, where M is a hermitian, unitary and anti-commutes with the perpendicular current density[13]. It can be generally given by[1]

$$M = \sin(\alpha)\tau_0 \otimes (\hat{n}_1 \cdot \vec{\sigma}) + \cos(\alpha)(\hat{\nu} \cdot \vec{\tau}) \otimes (\hat{n}_2 \cdot \vec{\sigma}) \tag{5}$$

where τ_i, σ_i are the Pauli matrices on sublattice space and momentum valley space respectively. $\alpha, \hat{\nu}, \hat{n}_1$ and $\hat{n}_2$ are parameters to be determined by the geometry and symmetries of the boundary, $\hat{n}_1$ and $\hat{n}_2$ are 3D unit orthogonal vectors that are orthogonal to the normal to the boundary. Forcing the time reversal symmetry $T = \tau_y \otimes \sigma_y K$ (where K is the conjugation operator) and particle hole symmetry ($\tau_z \otimes \sigma_z$) on the problem will reduce to two sets of boundary conditions

$$M = \pm\tau_z \otimes \sigma_z \text{ for zigzaz like BC } \quad \text{or} \quad M = \tau_z \otimes (n_x\sigma_x + n_y\sigma_y) \text{ for armchair like} \tag{6}$$

To avoid divergence, we assume that the amplitude of edge localized states will decay inside the dot. Therefore $\psi_{i-1,j+1} = \lambda\psi_{i,j}$ where i,j label the site located at $\vec{R}_{\text{ref}} + i\vec{a}_1 + j\vec{a}_2$ and $|\lambda| \leq 1$. It then follows from the tight binding model that $\psi_{i+1,j} = -(1 + \lambda)\psi_{i,j}$. Then assuming the boundary has some sort of periodicity over a translation vector $\vec{t} = n\vec{a}_1 + m\vec{a}_2$, then using the bloch theorem we obtain

$$\psi_{i+n+m-m,j+m} = \psi_{i+n,j+m}e^{ik} = (-1)^{n+m}(1 + \lambda)^{n+m}\lambda^m\psi_{i,j} \tag{7}$$

That is, $(-1)^{n+m}(1 + \lambda)^{n+m}\lambda^m = e^{ik}$ which will have discrete set of solutions (boundary modes) for each "quasi-wave" vector k.

The Dirac equation approximate states near the Dirac points around $k = 0$, it then follows that $(-1)^{n+m}(1 + \lambda)^{n+m}\lambda^m \in \mathbb{R}$, that is, for any solution λ_+ there is a conjugate solution $\lambda^*_+ = \lambda_-$, each one of the solutions will correspond to a different Dirac point $\{e^{+K\cdot r}, e^{-K\cdot r}\}$. Furthermore, there are two lattice points in the honeycomb lattice, so the boundary modes can be written using a Dirac Spinor of the form $[\psi^K_A \quad \psi^K_B \quad \psi^{-K}_B \quad \psi^{-K}_A]^T$, where each of the corresponding to the non-decaying wave vector solution. If the number of equations (missing sites) did not uniquely solve the equations one gets a degeneracy. And if the equations are sufficient for a unique solution then it is the trivial solution. Therefore, unless the number of missing sites are equal, two of the amplitudes will have to be zero ($\psi^K_A = \psi^{-K}_A = 0$ or $\psi^K_B = \psi^{-K}_B = 0$). Which given the conditions in6 will correspond to zigzag like boundary conditions.

Here we dealt with the edge of a terminated ribbon, but notice that we did not mention the other edge of the ribbon, while maintaining locality around the edges, therefore, the presented argument, and generally the work of[1] will be applicable to any large dot of any shape, which is supported by numerical calculations in[20] that we reproduced if figureD.3
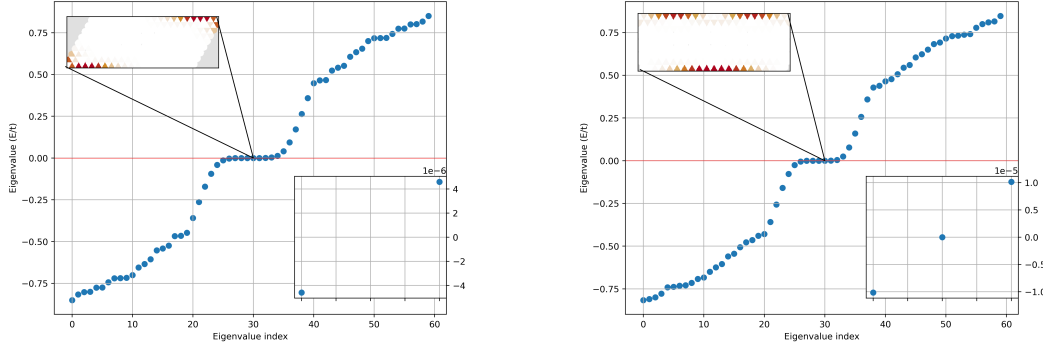
(a) Energy spectrum of a finite ribbon near fermi energy

(b) Energy spectrum of a finite rectangular flake near fermi energy

Figure 2.2: Energy spectrum of two finite quantum dots, the top left inset is the local density distribution, while the right bottom one include a zoom on quasi-zero energy states

2.3 Finite systems (Quantum dots)

As we have shown in the previous subsection, arguments given by[1] and[20] are not applicable unless the size of the dot is large $R \gg a$ (so that the local nanoribbon approximation is valid). For smaller dots, the Dirac effective mass model approximation is no longer useful. Therefore, we use numerical solutions to TB model using Kwant, and report on the existence of zero energy edge states. We confirm the results given in[7] that only triangular quantum dots with zigzag edges support degenerate zero energy localized edge states.

We begin by examining a finite version of the nanoribbon shown in2.1 near the fermi energy, we find similar findings to that of reference[7], but we find a single zero energy state in the rectangular shaped dots, with "rough edges" (see figure2.2b), All another tested shaped had no degenerate zero-energy eigenstates, yet as the size increases, the energy gap around the Fermi energy closes, with some dots acquiring quazi-zero energy eigenstates (like the nanoribbons in figure2.2a and circular and zigzag hexagonal quantum dots in figure2.3c &2.3i).

While none of the shapes in figures2.3 and2.2 have degenerate zero energy edge states, they still show quazi-zero energy eigenstates for larger dots, our simulations for the larger sized dots in figures2.3c and2.3i, where circular boundary behaves zigzag like, which confirms the results in[1] and[20]. In contrast, the energy gap around Fermi energy persists in the armchair edges dots even with bigger sizes (figures2.3f and2.3l). As shown in figure2.4, similar sized hexagonal dots will have close density of states, except for the finite density near Fermi energy.

2.3.1 Triangular zigzag quantum dots

An interesting geometry that pops out when considering the zero-energy edge states is the triangular zigzag shape. This geometry has the property that its edge consists of one type

(a) (b) (c)

(d) (e) (f)

(g) (h) (i)

(j) (k) (l)
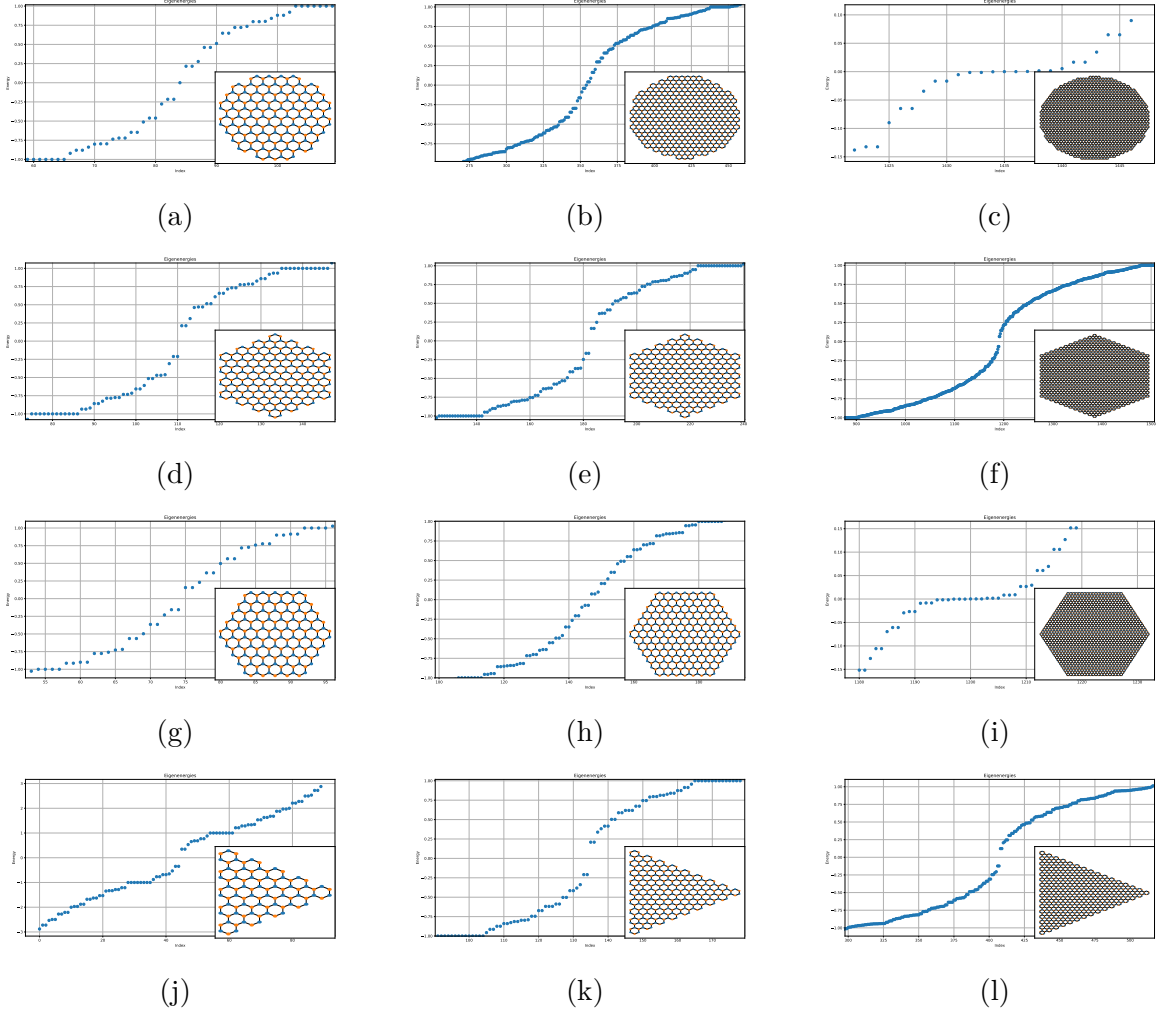
Figure 2.3: energy levels of different shapes and sizes of honeycomb quantum dots

6
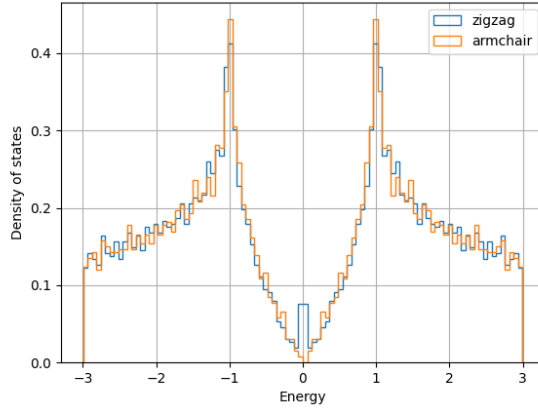
Figure 2.4: Density of states of armchair hexagonal dot compared to that of zigzag hexagonal dot of roughly the same size ($r = 27a$). The armchair edged dot clearly lacks zero-energy states compared to the zigzag counterpart.

(a) (b) (c)
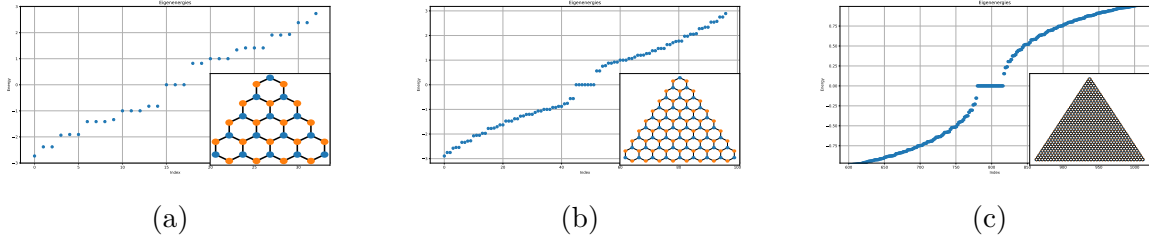
Figure 2.5: Energy spectrum of a triangular zigzag quantum dot with $N_{\text{edge}} = 4, 8$ and 38

of lattices, therefore, zero energy modes cannot keep the sublattice symmetry, and will be localized on one of the sublattice.

As a result of this special geometry, a triangular quantum dot with N_{edge} sites at the edge will have $N_{\text{edge}} - 1$ degenerate zero energy eigenstates. Even for arbitrary small sizes[3]. Therefore, only infinite systems (like nanoribbons and large dots (disks)) and zigzag triangular quantum dots have degenerate zero energy eigenstates (figure 2.5). While most of the eigenstates are localized at the edges, some are not, and are delocalized over the whole dot. This is shown in figure 2.6d&2.6e. Yet despite this delocalization, edge states are still dominant. The high density of states at the Fermi energy is a special property of the triangular zigzag geometry.

2.4 Symmetry breaking

The effect of symmetry breaking on the edge states of general honeycomb quantum dots with zigzag-like boundaries was reported in[20], here we will focus on the unaddressed case of triangular zigzag quantum dots and armchair quantum dots. We investigate the effect of breaking the time reversal and sublattice symmetries. Time reversal symmetry is usually broken by applying a magnetic field, while sublattice symmetry could be effectively broken

(a)

(b)

(c)

(d)

(e)
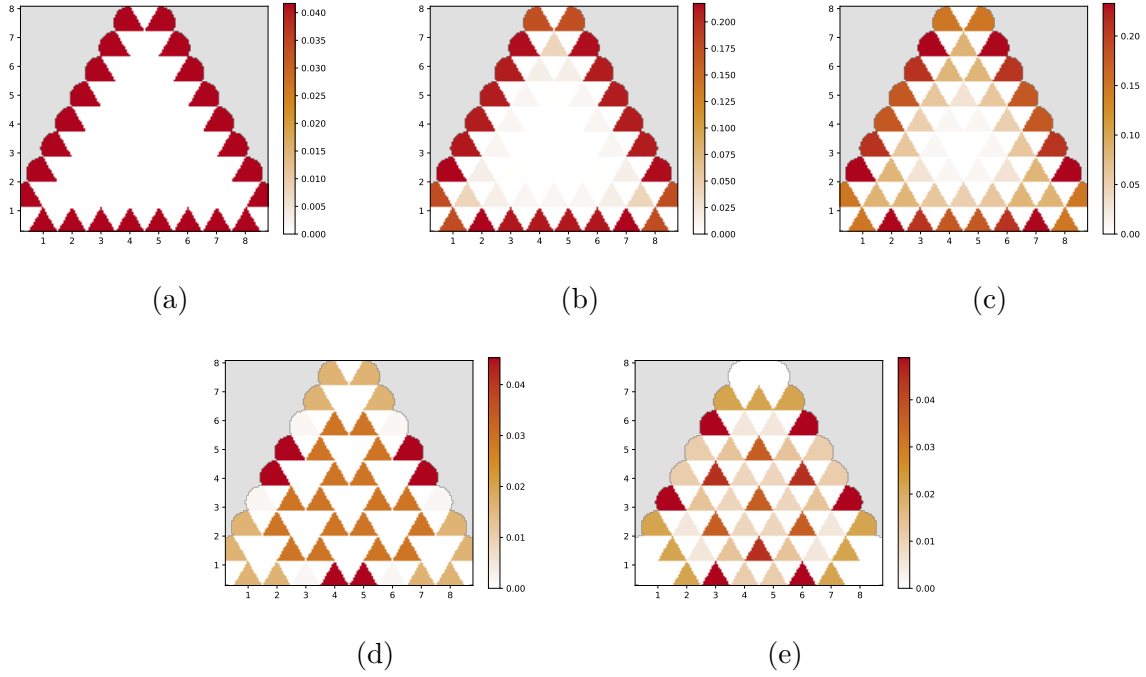
Figure 2.6: local density of zero energy eigenstates, rather than diagonalizing the zero energy degenerate subspace with respect to the rotation operator, then with one that is symmetric around the central axis. We broke the symmetry by a tiny second-nearest neighbor hopping term $1 \times 10^{-12}t$ which effectively diagonalized the states with respect to the symmetric operators. These results reproduced those of[3]
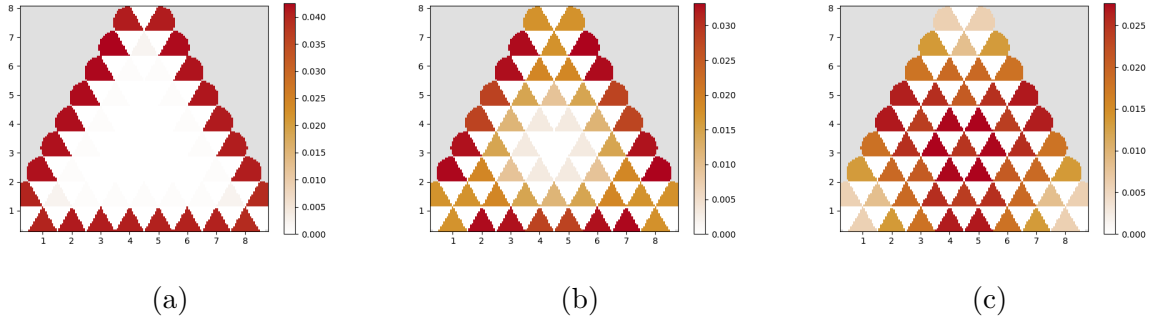
Figure 2.7: Effect on local density of states for a magnetic perturbation ($B = 0.1$) on a triangular zigzag quantum dot. These are edge states corresponding to 2.6a, 2.6c and 2.6e

by adding real next nearest neighbor hopping terms.

For the triangular zigzag quantum dots, we find that the edge component edge states are robust against applied magnetic fields, while the bulk part of the states that are further away from the edges are will have increased local density (figure 2.7).

As the magnetic field increases, new states will be pushed towards the zero energy (zeroth landau level), those states are not edge localized in general, their density depend on the cycletron radius which is inversly proportional to magnetic field. When the bulk component of the edge modes gradually increase (figure 2.7).

As for the effect of sublattice symmetry breaking on the triangular zigzag dot apart from breaking the degeneracy of the zero energy states based on the ratio of sites on the edges, we find that sites that are fully localized at the edges (such figure 2.6a) are the least effected in terms of energy (shifted exactly by $2t'$). This agrees with the results in [20] and [1], where it was shown that second-nearest neighbor hopping on the edge states is equivalent to adding staggered potentials to the edges of the lattice, effectively shifting single electron energy (see figures D.2 and D.3).
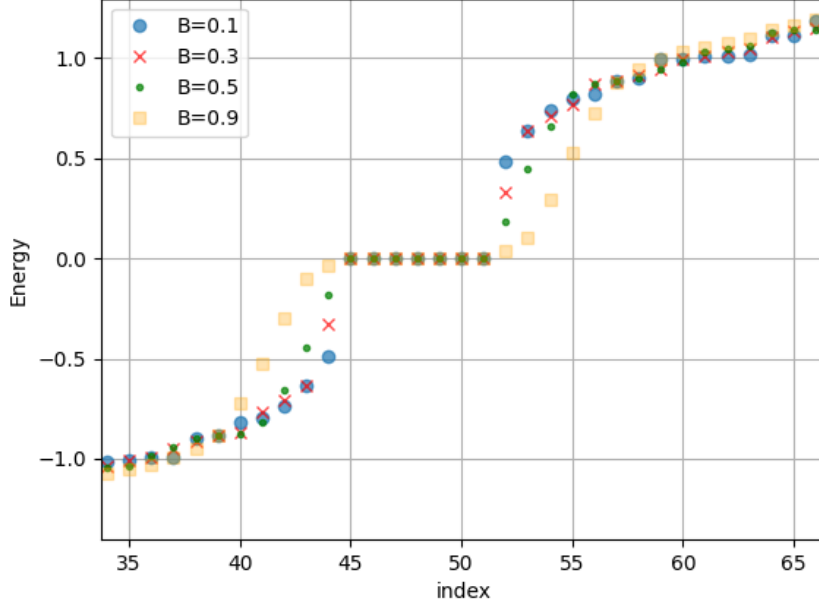
Figure 2.8: The effect of increasing magnetic field on energy modes near $E = 0$.

3 Quantum Spin Hall effect and Topological Insulators

In this section we will discuss the quantum hall effect and its variations on the honeycomb lattice. Graphene is known for realizing unconventional quantum hall effect due to its relativistic properties[9]. Due to the large separation between its landau levels it is able to maintain quantum hall edge states even at room temperature (under high magnetic fields). Based on these interesting properties, we examine the possibility of realizing topological quantum spin hall (QSH) states in small graphene-like systems, and how different geometries might impact the edge states.

Kane and Mele predicted that QSH effect can exist in graphene nanoribbons[11] when taking spin orbit coupling into account. While we understand that it is not realistic to adjust the spin orbit coupling as a tunable parameter. We still find it insightful to study its effect and how it comes into play in different geometries.

We begin by measuring the effect of spin orbit coupling on infinite nanoribbons. We find that the edge states are effectively "pumped" from one edge to the other, thinking of this as pumping charges is what will later define the topological invariant.

3.1 Topological Invariant

The topological invariant that is used to characterize the QSH effect is the $\mathbb{Z}_2$ invariant. However, we will rather deal with another related invariant, the Chern number, which is used to characterize the quantum hall effect in the Haldane model. We will assume the system to be in spin polarized state, and effectively study one "half" of the QSH state. In order to define the Chern number, we need to define a Berry connection and curvature, which
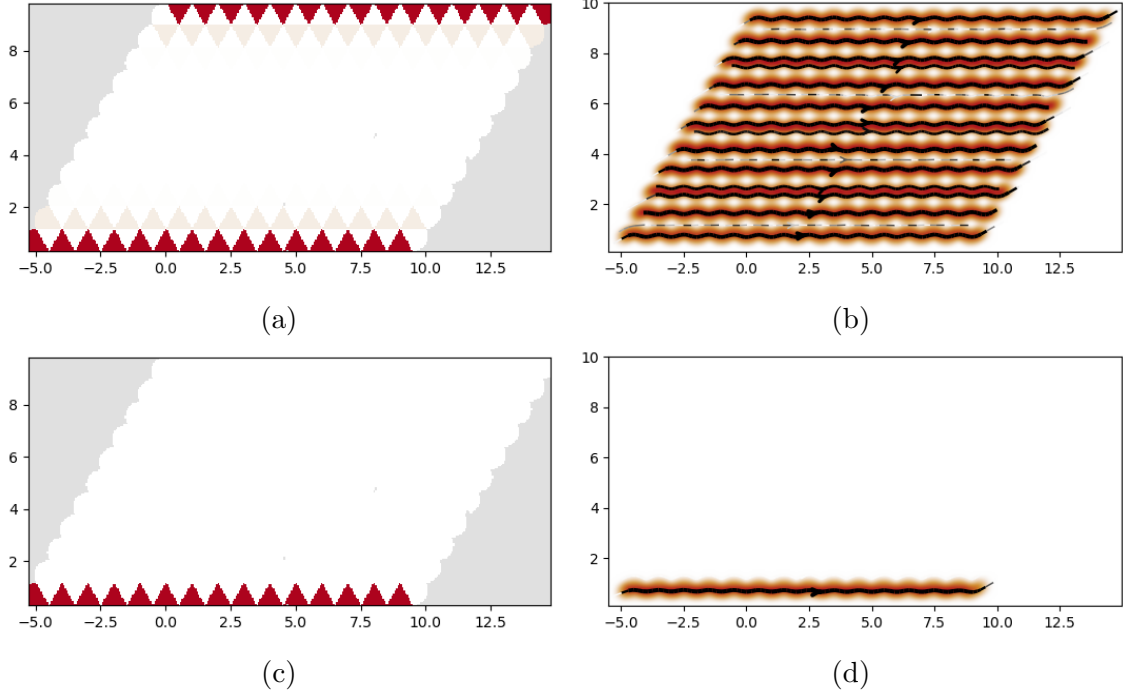
Figure 3.1: The effect of spin orbit coupling on the edge states of a nanoribbon. The left column the local density of states. While the right column is the current density. The top row is for $t_{SOC} = 0$ and the bottom row is for $t_{SOC} = 0.01$.

are related to the Berry phase and the adiabatic theorem, which reads as[21]

$$\left| \psi_n(\vec{R}(t)) \right\rangle = \exp\left(i\gamma_n(\vec{R}(t)) \right) \exp\left(-i \int_0^t \varepsilon_n(\vec{R}(t'))dt' \right) \left| n(\vec{R}(0)) \right\rangle \tag{8}$$

where $\vec{R}$ is a vector in the parameter space, ε_n is the instantaneous energy of the instantaneous eigenstate $\left| n(\vec{R}(t)) \right\rangle$, and γ_n is the Berry phase. The Berry phase is often set equal to zero, that why in many resources one finds the adiabatic theorem without the Berry phase term[14]. The Berry connection is then defined as

$$\mathcal{A}_n(\vec{R}) = i\hbar \langle n(\vec{R}) | \frac{\partial}{\partial \vec{R}} | n(\vec{R}) \rangle \tag{9}$$

Then the Berry phase is defined as

$$\gamma_n(\vec{R}) = \oint_c \mathcal{A}_n(\vec{R'}) \cdot d\vec{R'} \tag{10}$$

Where c is a contour extending over the first Brillouin zone. It is clear from the above definition that the Berry phase is a geometric property that does not depend on time. The berry phase is a gauge invariant, while the Berry connection is not. Therefore, another gauge invariant "the Berry curvature" is defined as in analogous way to the magnetic field

$$\Omega(\vec{k}) = \nabla_{\vec{k}} \times \mathcal{A}(\vec{k}) \tag{11}$$

11

Which in this case the Berry phase will become a surface integral over the first Brillouin zone, the berry phase could be then shown to take on values of integer multiples of 2π, this integer coefficient is the Chern number (W), which is a topological invariant.

$$W := \frac{1}{2\pi} \iint_{\text{BZ}} \vec{\Omega}(\vec{k}) \cdot d\vec{S} \tag{12}$$

Here we do not go over details for how the berry curvature is linked to the current and pumped charges, such derivations are provided in details in[21]. When the system is gapped, the Chern number is non-zero, and the system is in a topological phase. When the spin-orbit coupling is not strong enough to gap the bulk, the Chern number is zero, and the system is in a trivial phase (figure3.2). Another way to see this is that, is by adding a staggered potential to the system and tuning it, staggered potentials effectively open or closes the gap in the bulk, therefore forcing a topological phase transition. In figure3.2 we solve the hamiltonian13

$$H = -t \sum_{\langle i,j \rangle} c_i^\dagger c_j + (t_2 + it_{\text{SOC}}) \sum_{\langle\langle i,j \rangle\rangle} c_i^\dagger c_j + \sum_i (\pm m) c_i^\dagger c_i \tag{13}$$

Where $t_2, t_{\text{SOC}} \in \mathbb{R}$, the imaginary part incorporates the spin orbit coupling according to Kane-Mele model[11][3]. The sign in $\pm m$ is determined by the sublattice type.

3.2 Open systems

We have discussed the edge states of finite systems, here we will discuss how whether they are topological or not. The problem with finite systems with open boundary conditions is that the Chern number that identifies the topological bulk is not well-defined, because the definition12 requires integrating over the reciprocal space. We therefore resort to different equivalent topological invariant that is calculated in real space.

3.2.1 Bott index

The Bott index is a topological invariant that is equivalent to the Chern when defined over real space with periodic boundary conditions[17][10]. We therefore extend this definition to finite systems with open boundary conditions as in[10], with the distinction that we here calculate it for small crystals rather than quasi-crystals. The Bott index is defined by:

$$\mathcal{B} = \frac{1}{2\pi} \text{Im} \Big\{ \text{tr} \Big[\log \Big(e^{2\pi i PXP} e^{2\pi i PXP} \big(e^{2\pi i PXP} \big)^\dagger \big(e^{2\pi i PXP} \big)^\dagger \Big) \Big] \Big\} \tag{14}$$

Where X, Y are the normalized diagonal position operators defined and P is the Fermi projection operator, defined as the sum of outer product of occupied states $\sum_{i \in \text{occ}} |\psi_i\rangle \langle\psi_i|$

3.3 Spin orbit coupling on finite systems

The spin-orbit coupling effect is known to introduce gaps to the gapless graphene energy bands, but for finite systems, the spin orbit coupling has the effect of "linearizing" the
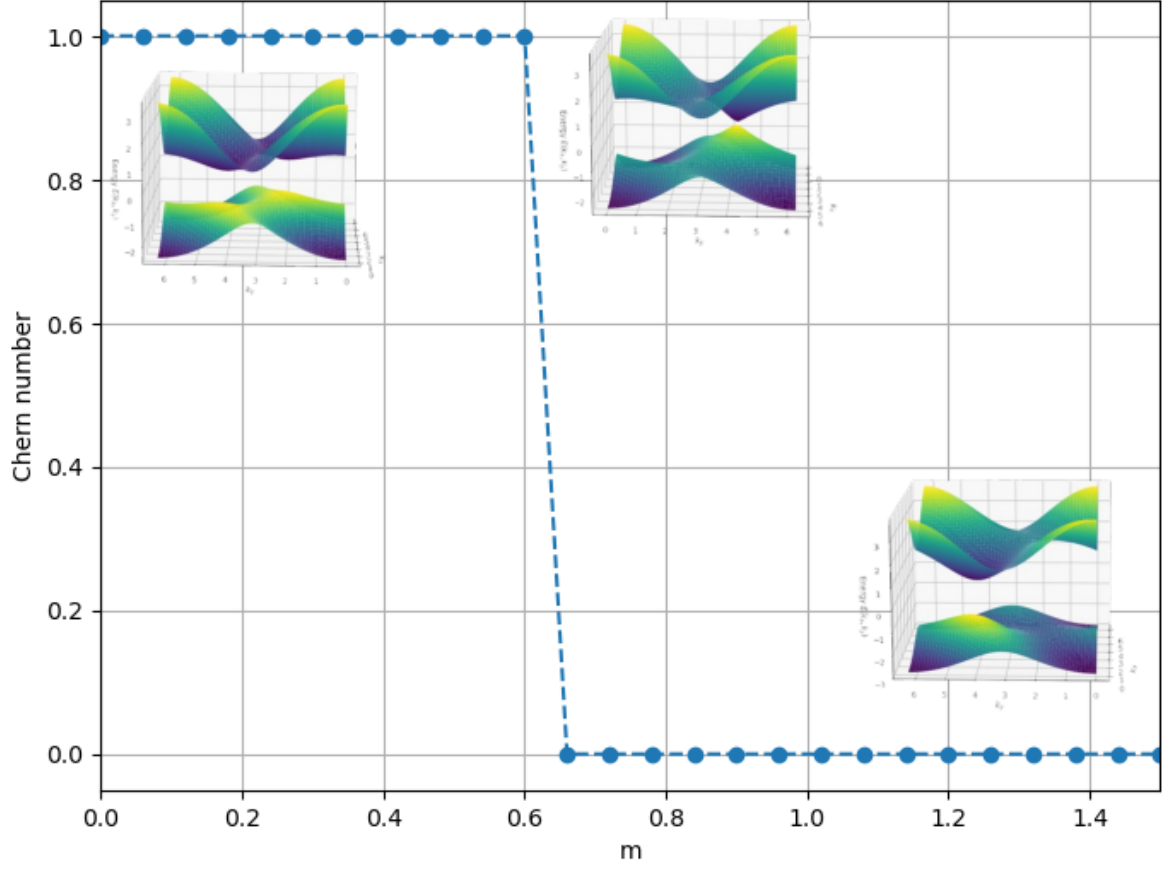
Figure 3.2: The Chern number as a function of the staggered potential m, with a second-nearest neighbor hopping $t_2 = 0.15e^{i\pi/3}$. The insets show the energy bands of the bulk, as m approaches the transition point, the bulk gap closes and the Chern number changes from $W = 1$ to $W = 0$. Our results match the calculations by[10]

energy states near the Fermi energy. These new linearized states are more edge localized towards the Fermi level, and spread more inside the bulk of the dot as we move away from the Fermi energy.

Another important feature to notice when dealing with the edge states is their distribution around the edge. In order to realize the QSH effect, edge states should be spread over the whole edge, and not localized on few edge sites. This is necessary in order to have propagating spin polarized propagating states (they should be conductive). In section2.3 we showed that metallic edge states are only realized in large dots, or in zigzag triangular quantum dots, where they will be distributed over the whole edge (figure2.5). And even in the bigger sized dots, edge states tend to localize on the zigzag parts, while the armchair parts are generally empty[20]. However, when spin orbit coupling is added, the aforementioned emerging edge states will be delocalized over the whole edge, even armchair ones (see figure3.3).

There are multiple ways to add spin orbit coupling to the system, one requires adding hopping terms to the confined (S, Px, and Py) orbitals and tuning the hopping parameters[3]. Another requires adding an effective imaginary hopping term to the second nearest neighbor hopping[11]. Since the results are proved to be semilar, and the second method is easier to implement, and computationally cheaper, we will use it in our simulations. The hamiltonian of the system will be given by

$$H = -t \sum_{\langle i,j \rangle} c_i^\dagger c_j \sigma_0 + \sum_{\langle\langle i,j \rangle\rangle} \left[t_{2ij}\sigma_0 + it_{\mathrm{SO}}\sigma_3 \right] e^{i\phi_{ij}} c_i^\dagger c_j + \sum_i (\pm m) c_i^\dagger c_i \sigma_0 \tag{15}$$

The mass term will be used to change tune the gap in the bulk, and transition between topological and trivial phases. $e^{i\phi_{ij}}$ is a Peierls phase factor to add the magnetic field, ϕ_{ij} is zero unless otherwise stated. $\{\sigma_i\}$ are the Pauli matrices.

In section2.3 we showed the existence of zero energy edge states in triangular zigzag quantum dots (TZQD) of arbitrary sizes. We find that even SOC breaks the degeneracy of TZQD's zero energy states. Even a small perturbation of the SOC will be sufficient to form similar states to those in figure3.3 on the edges of the TZQD. Higher spin orbit coupling will lead to a more edge-localized states, and will decrease the bulk states (figure3.5).

3.4 Quantum spin hall states in small Dots

Following what we did in section3.1 for the infinite systems, we aim here to observe topological transition in the finite dots systems. This could be tricky because here the gap is always closed, as the edges are always considered in our small sized systems. By calculating the Bott index, and the spin-polarized conductance we aim to determine how size affect the QSH effect in small open systems.

There are few key features that identify the QSH effect. Either a plateau in the spin-polarized conductance. Another is the Bott index, and also the local density of states and spin-polarized local current density.
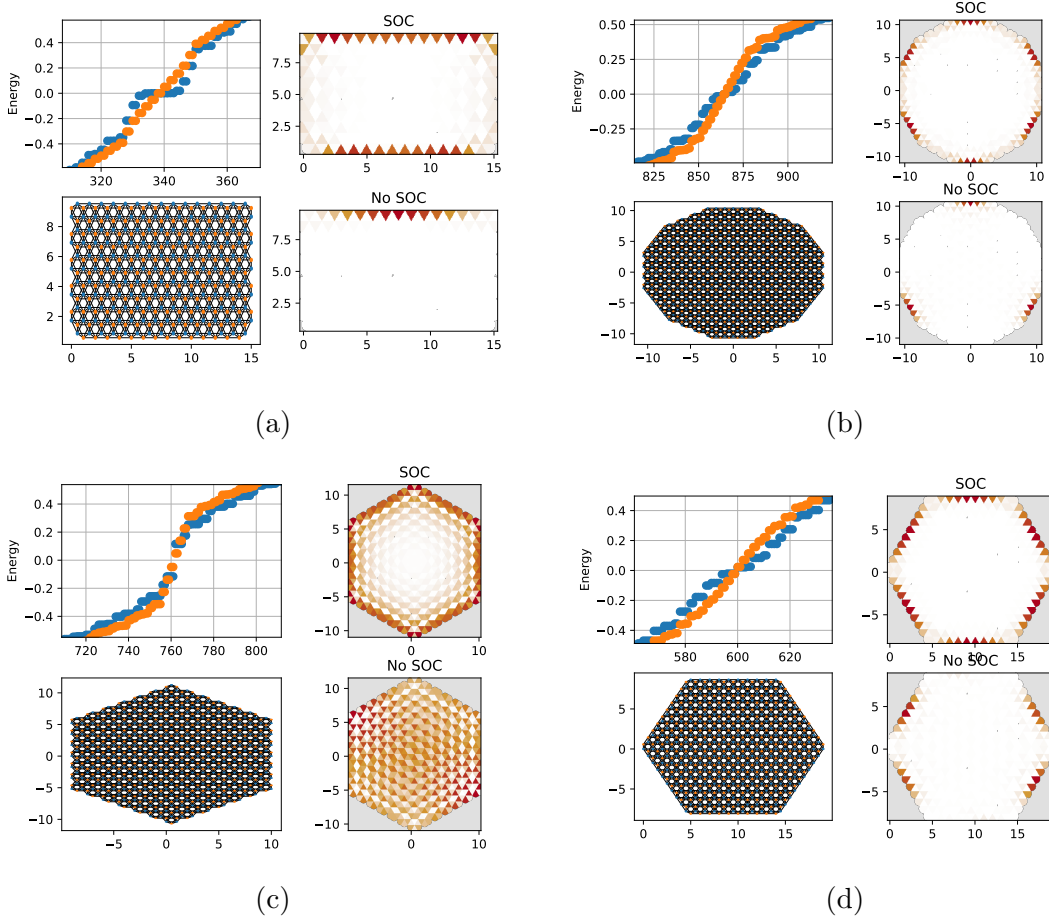
Figure 3.3: The effect of spin orbit coupling on the state closest to Fermi energy for different shapes of quantum dots.
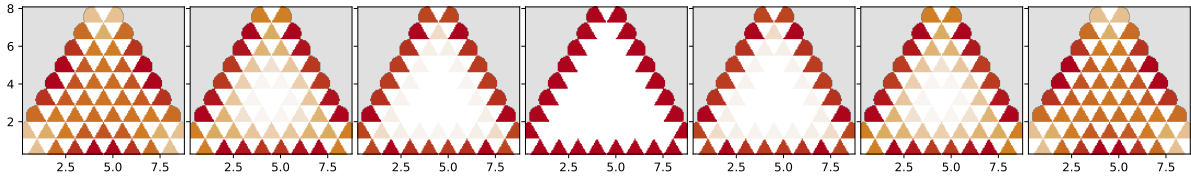

Figure 3.4: The effect of spin orbit coupling perturbation ($t_{\mathrm{so}} = 10^{-12}t$) on the metallic zero energy states in (TGQD).
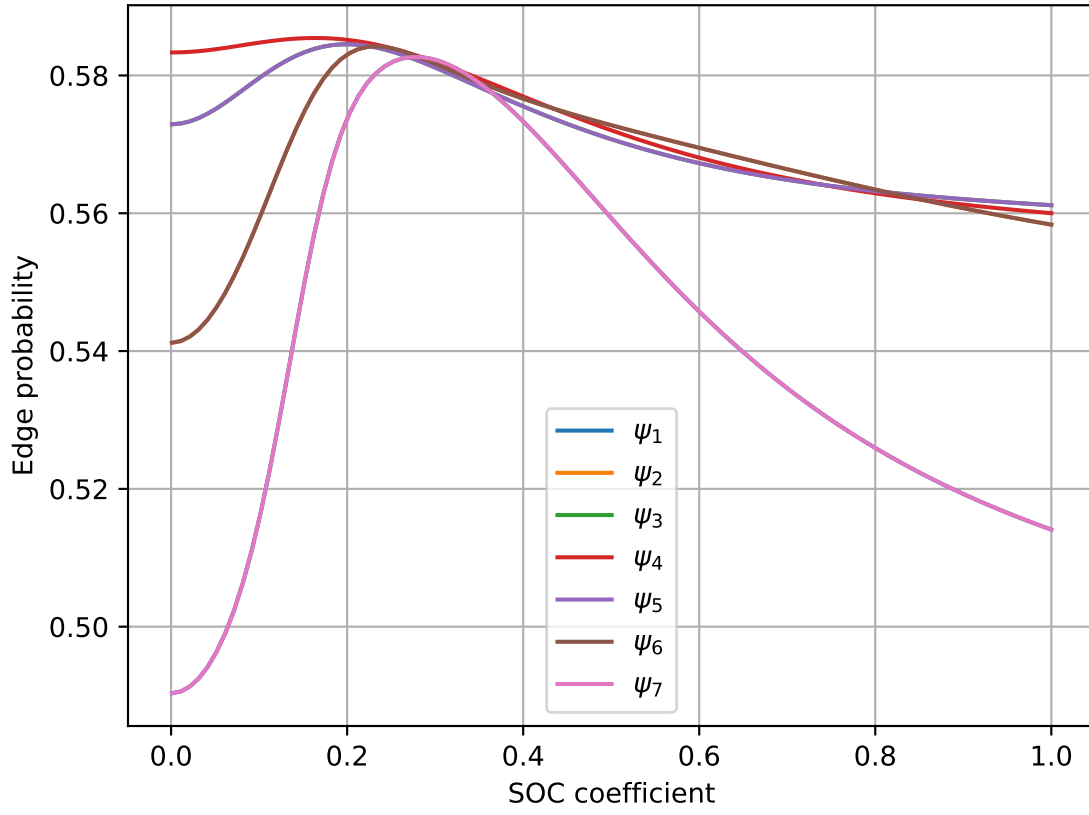
Figure 3.5: The effect of spin orbit coupling on the edge states of a TZQD, with higher coupling coefficient, the edge states probability increases. The order is the same as that shown in figure 3.4
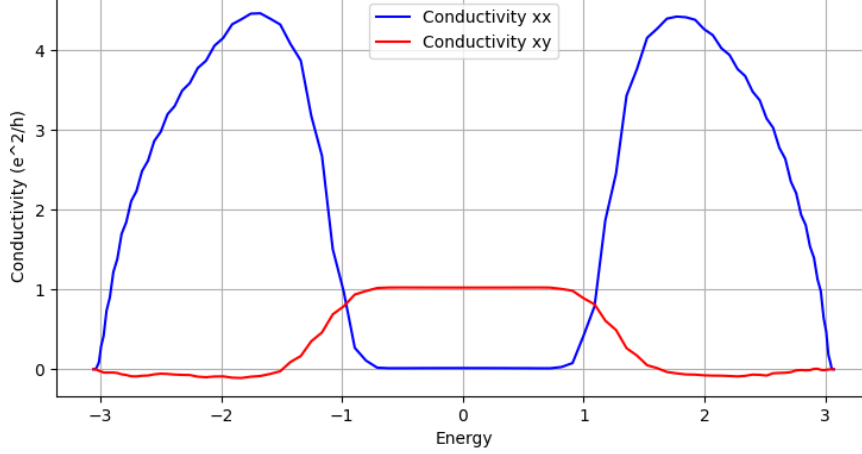
Figure 3.6: Spin-polarized conductance of a large triangular quantum dot with zigzag edges ($N_{\text{edge}} = 23$) using KPM. The plateau at $G = 2e^2/h$ ($G = e^2/h$ for each spin polarization) is a signature of the QSH effect.

3.4.1 Spin-polarized Kubo conductivity

Here we will make use of the kernel polynomial method (KPM)[19] to calculate the spin-polarized Kubo conductivity of the system. The KPM is a numerical method that allows us to calculate the density of states and the conductance of the system without diagonalizing the Hamiltonian. It is typically used to calculate the density of states of large systems, but it can also be used to approximate the behavior of the bulk using the correct parameters. We use the implementation in the Kwant package[8] and keep the sampling vectors in the center of the dot to capture the bulk conductivity. While using this method we keep in mind that it has a convergence condition proportional to $1/\sqrt{DN}$, where D is the system size and N is the number of vectors used to approximate the expectation values. For the smaller dots this approach is tricky, the smaller system sizes require more vectors, yet those vectors are not eigenstates so they introduce noise in the results, to the point where plateaus are not distinguishable. With that being said, we find good convergence for larger quantum dots (still less than 10nm in size), with a clear Hall plateau at $G = 2e^2/h$ for the spin-polarized conductance that also corresponds to 0 longitudinal conductance (see figure3.6).

3.4.2 Local density of states and local current density

A characteristic of the QSH effect is the presence of edge states that are spin-filtered with chiral propagation in opposite directions. Furthermore, these edge states are expected to be robust against perturbations and disorders. As long as they obey TRS We therefore calculate the local density of states (LDOS) and the local current density (LCD) of "injected" electrons to observe the edge states. We start with the Kane-Mele models' hamiltonian15, with real next nearest neighbor hoppings and magnetic field added using Peierls substitution and random onsite disorder

$$H = -t \sum_{\langle i,j \rangle} \exp\left(i\frac{e}{\hbar}\Phi_{ij}\right) c_i^\dagger c_j + (t_2 + it_{\text{soc}}) \sum_{\langle\langle i,j \rangle\rangle} \exp\left(i\frac{e}{\hbar}\Phi_{ij}\right) c_i^\dagger c_j + \sum_i \left(\pm m + W_{ij}\right) c_i^\dagger c_i \quad (16)$$

Where $\Phi_{ij} = \int_{\vec{r}_j}^{\vec{r}_i} \vec{A}(\vec{r}) \cdot d\vec{\ell}$, and W_{ij} is a noise term. The procedure to calculate the local current density is provided in appendix B. In this section we plot the local current density for a rectangular quantum dot. Which will be further investigated in section 3.4.3.

3.4.3 Bott index for small dots

In section 3.1 we introduced the Bott index as a topological invariant that is equivalent to the Chern number in periodic systems. We will use it here to characterize the topological phase of small quantum dots. This will be done by tuning the staggered potential parameter (m in equation 15) (when the system switches from 1 to 0). The Bott index is defined originally for periodic systems and torus geometries (so that x and y coordinates are mapped to angle θ and ϕ). While it was shown to have been calculated for systems with different topologies (here topology is meant in a geometric sense). We found some unexpected results for triangular shapes, where the Bott index is 0 for all sizes and all values of m. Therefore, we restrict our analysis here to different shapes can obey the torus topology like the rectangular shape.

We first notice that the Bott index has a size and shape dependencies, topological transition occurs at smaller values of m for smaller sizes (we will refer to this term as "critical mass" m_c). Large systems will approach the Chern number calculations we did in section 3.1 (see figures 3.8 and 3.9). While we also note that the topological behavior of quantum dots is more affected by the zigzag edge compared to the armchair one, that is, zigzag edges contribute more to the topological properties of the system (compare red and blue curves in figure 3.9).

### 3.4.4 Two terminal conductance

In section 3.4.1 we used the KPM to calculate Kubo conductivity for a quantum dot. Yet for Finite systems with open boundary conditions, the Kubo conductivity is sensitive to edge effects, thus not suitable for small systems (the KPM also divergence for smaller systems). Another way to calculate the conductance of a finite system is to use the landauer-Büttiker formula, which defines the conductance as a scattering problem. Assuming the two leads to be held at chemical potentials $\mu = \{-V/2, V/2\}$. The current through the system is given by

$$I = \frac{e^2}{h} \int \sum_{n=1}^{N} T_n(E) \left(f(-V/2 + E) - f(V/2 + E) \right) dE \tag{17}$$

$$I = \frac{e^2}{h} \int_{-V/2}^{V/2} \sum_{n=1}^{N} T_n(E) dE \quad T \approx 0\text{K} \tag{18}$$

$$\frac{dI}{dV} = \frac{e^2}{h} \sum_{n=1}^{N} \frac{T_n(V/2) + T_n(-V/2)}{2} \tag{19}$$

$$G = \frac{e^2}{h} \sum_{n=1}^{N} T_n \quad \text{at Fermi energy } \mu \tag{20}$$

18
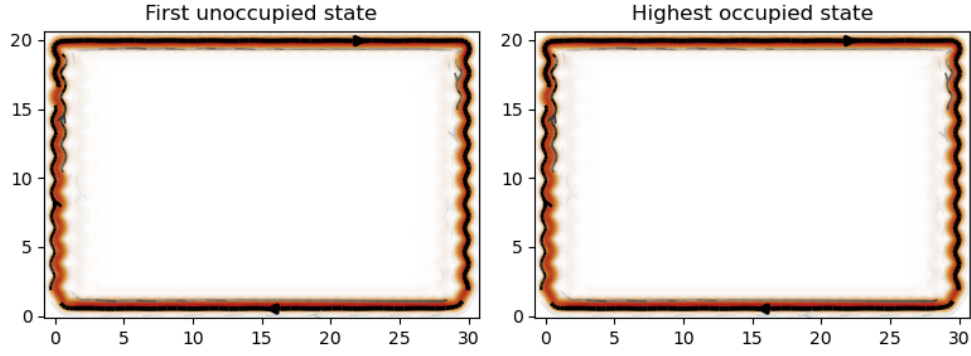
(a) Local current density $m = 0.0$
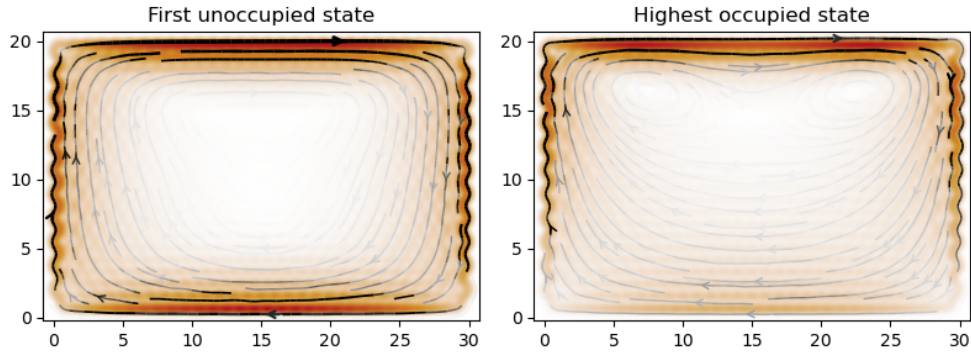
(b) Local current density $m = 0.55$
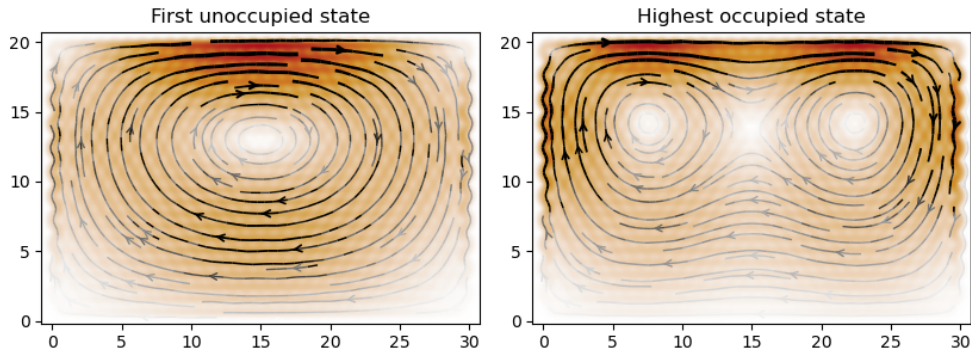
(c) Local current density $m = 0.75$

(d) Local current density for a rectangular quantum dot with diminsions 30×20. The local current density is calculated for a single electron state. The figure shows a transition between edge localized states to bulk states.
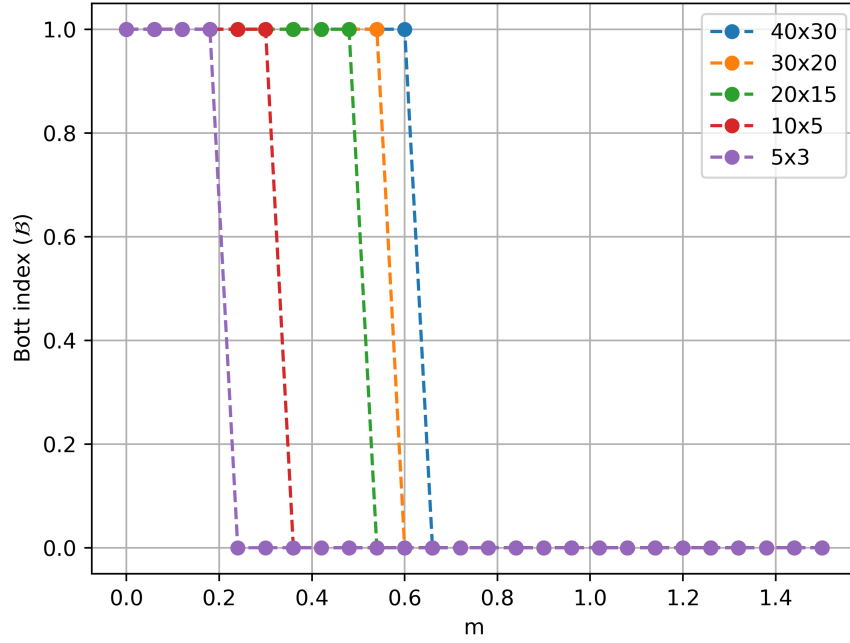
Figure 3.8: The Bott index as a function of the staggered potential m for different sizes of rectangular quantum dots. The topological transition occurs at smaller values of m for smaller sizes. Notice for 40×30 rectangular dot that we retrieve the chain number in figure3.2
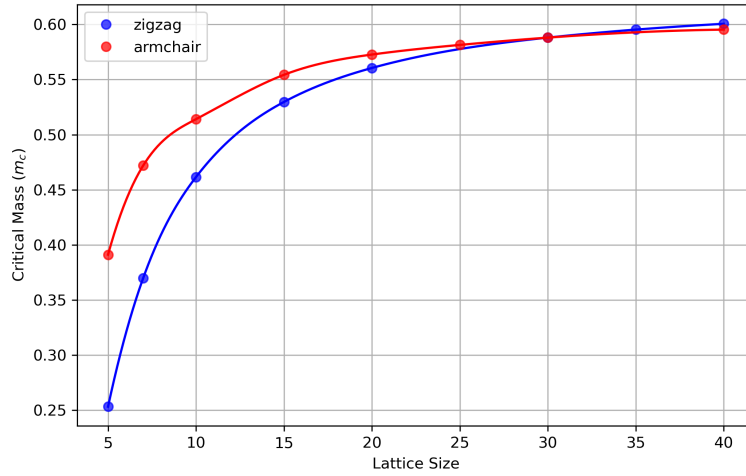
Figure 3.9: The critical mass m_c as a function of the size of the rectangular quantum dot (zigzag edge $L_y = 30$ is fixed in blue curve, while the armchair edge is fixed for the red curve).

Where T_n is the transmission coefficient of the nth mode for the incoming electron. Since we are studying quantum dot, we would like to keep these leads minimal (single chain of atoms) to avoid any notable effects on the quantum dot system. Following the model proposed Sivan and Imry in[15] for the quantum hall effect. We apply similar ideas to the quantum spin hall effect. The edge states are treated as a 1D system with two junctions (contact with leads). Assuming symmetry between junctions, and in the absence of magnetic fields, the transmission coefficient is given by

$$T = \frac{|t|^2}{1 + |r|^2(1 - 2\cos(kP/t_{\text{SOC}}))} \tag{21}$$

where P is the dot's perimeter, k is the wave vector of the incoming electron, $|t|^2, |r|^2$ are the transmission and reflection coefficients of each junction. We clearly see that the conductance will have oscillations in the energy space, with a frequency that is proportional to the system perimeter. According to this simplistic model, the transmission coefficient will have oscillations with respect to the SOC coefficient and to the system size. Unlike in the quantum hall effect case in[16]. We do not have Aharonov-Bohm-like oscillations here due to the absence of magnetic field. We also find a dependence of the amplitude of the oscillations on the SOC coefficient (figures3.10 and3.11). Furthermore, we notice that for a range of SOC coefficients after $t_{\text{SOC}} \approx 0.2$ the transmission and conductance becomes size independent, with larger dots maintaining quantization for even higher SOC coefficients.

In figures3.10c,3.10d,3.11c and3.11d. We show that the transverse spin polarized conductance is quantized with the oscillations averaging to $G \approx e^2/h$. In the limit of infinite system size, these oscillations will converge to the quantized value.

3.4.5 Staggered potential and next nearest neighbor hopping

The quantum spin hall effect is sensitive to the staggered potential as we show in figure3.2 since it opens a bulk gap. When the staggered potential is increased, we observe higher oscillations in higher energies, and the oscillations starts increasing until the quantum spin hall states are completely suppressed. These highly oscillating states resembles the transport through the bulk. A similar effect is observed when the real part of the next nearest neighbor hopping is increased. Since the staggered potential and the nnn-hopping both have similar impacts on the system, they can also be used to cancel each other's effect to some extinct, this works well for when the edge states are edge localized, yet in the trivial phase this cancellation will not work (figure3.13).
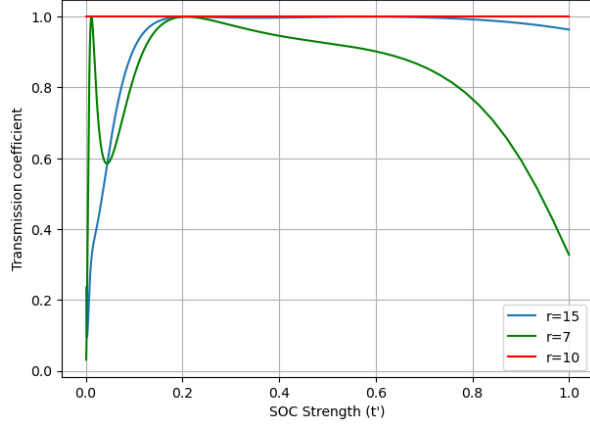
(a) Transmission coefficient as a function of the SOC coefficient at $E = 0$ for three different sized circular quantum dots.
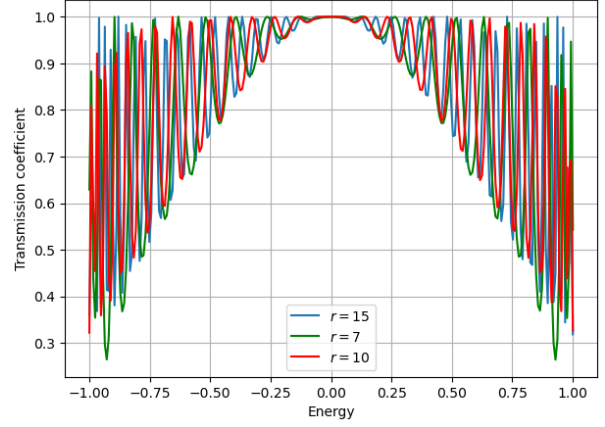
(b) Transmission coefficient as a function of energy for three different sized circular quantum dots.
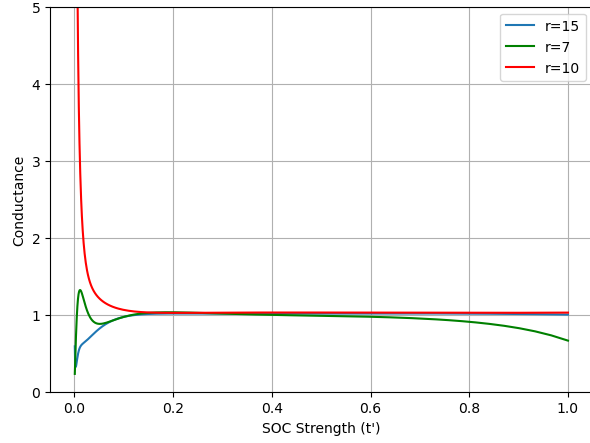
(c) Spin Hall Conductance as a function of the SOC coefficient at $E = 0$ for three different sized circular quantum dots in units of e^2/h.

(d) Spin Hall Conductance as a function of energy for three different sized circular quantum dots in units of e^2/h.

Figure 3.10: Comparison of transmission and conductance as a function of SOC coefficient and energy for three different sized circular quantum dots. Notice the total transmission and quantization of the QSH conductance.
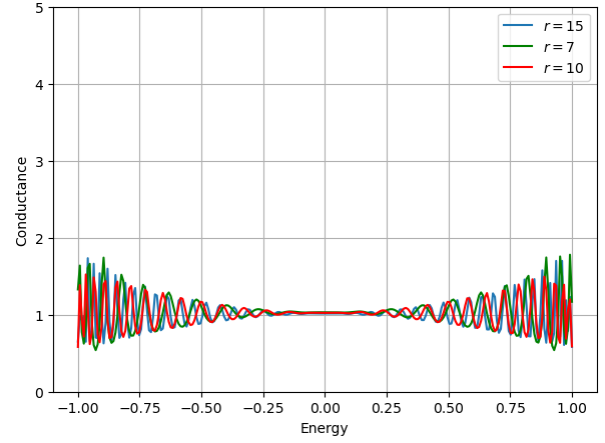
(a) Transmission coefficient as a function of the SOC coefficient at $E = 0$ for two different sized circular quantum dots.

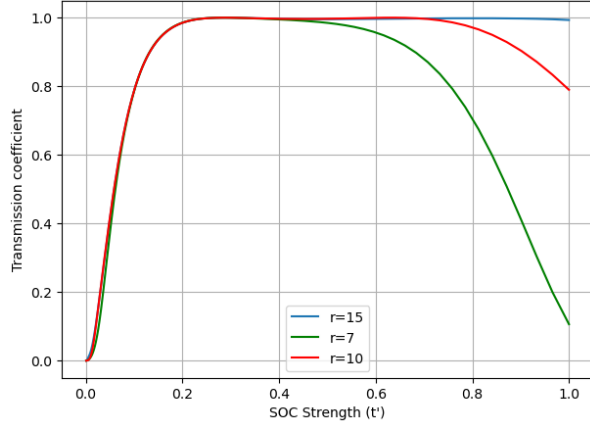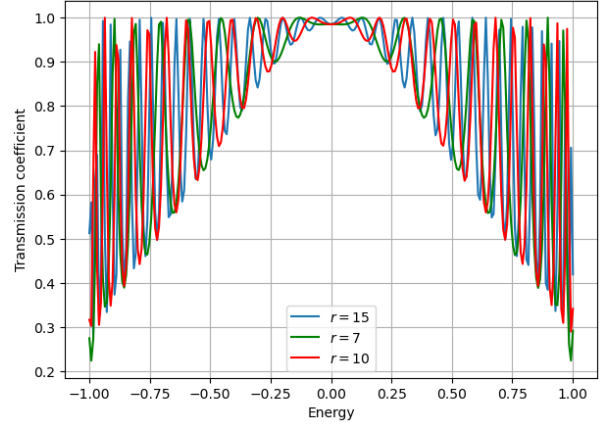(b) Transmission coefficient as a function of energy for two different sized circular quantum dots.
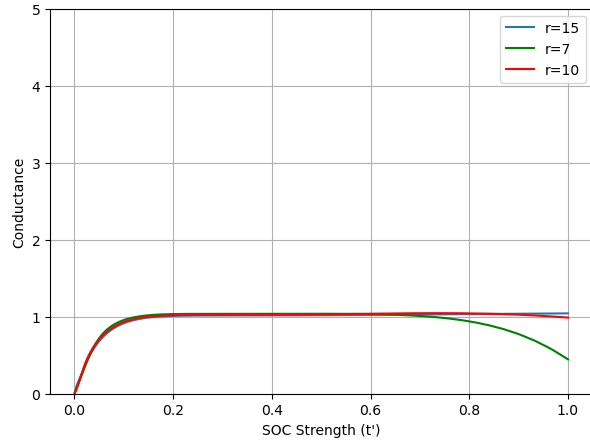
(c) Spin Hall Conductance as a function of the SOC coefficient at $E = 0$ for two different sized hexagonal zigzag quantum dots in units of e^2/h.
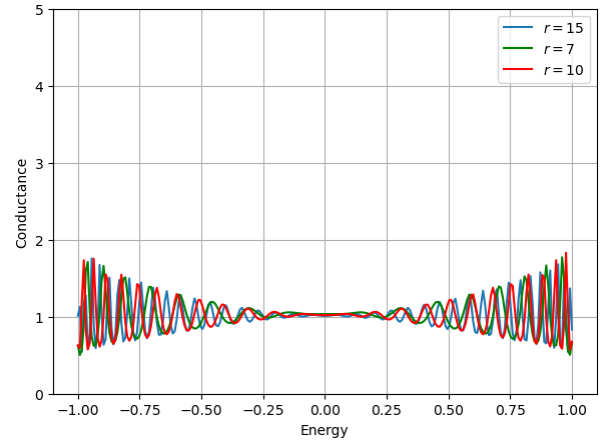
(d) Spin Hall Conductance as a function of energy for two different sized hexagonal zigzag quantum dots in units of e^2/h.

Figure 3.11: Similar to figure 3.10 but for hexagonal zigzag quantum dots
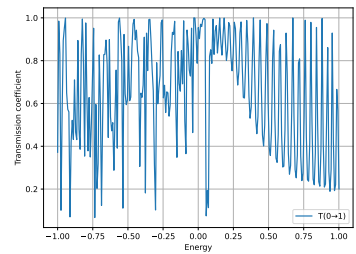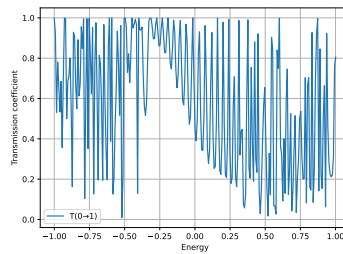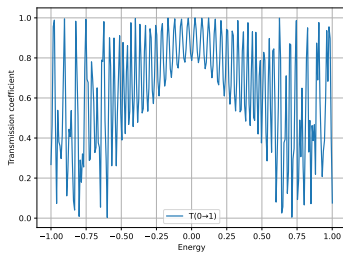
(a) $t' = 0.1$, $t_2 = 0.0$, $m = 0.0$ (b) $t' = 0.1$, $t_2 = 0.0$, $m = 0.2$ (c) $t' = 0.1$, $t_2 = -0.2$, $m = 0.0$

Figure 3.12: The effect of the staggered potential and real nnn-hopping on the spin polarized conductance of a large hexagonal zigzag quantum dot. The oscillations are more pronounced at higher energies, and the conductance is suppressed as the staggered potential is increased.

23
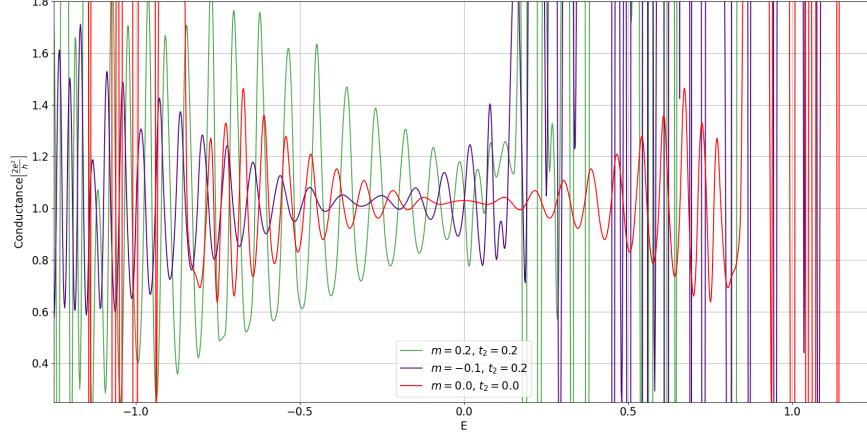
Figure 3.13: The effect of the staggered potential and nnn-hopping on the spin polarized conductance of a small circular quantum dot $r = 10a$. The oscillations are more pronounced at higher nnn-hopping $\Re(t_2)$, and the conductance is suppressed as the staggered potential m is tuned.

4 Conclusion

In the first part of this work we studied the edge states of small graphene-like quantum dots, and how they are affected by the geometry of the dot. We confirmed that triangular zigzag quantum dots and large sized dots have metallic edge states, while armchair quantum dots have insulating edge states that persist even for large sizes.

The second part of this work was dedicated to the quantum spin hall effect in small quantum dots. We reviewed the topological invariant of the quantum spin hall effect in order to test the topological properties of edge states discussed in the first part. We calculated the spin-polarized conductance and the Bott index for small quantum dots. It was found that the Bott index is size dependent, and that smaller sized systems have "weaker" topological properties that are easier to break. We also found that the Bott index is sensitive to the edge type, where zigzag edges contribute more to the topological properties of the system. Furthermore, we demonstrated the need for an invariant that is defined for finite systems that do not map to torus topology used in the Bott index.

Our conductance calculations found that while the average spin-polarized conductance is quantized at $G = 2e^2/h$ (e^2/h for each spin polarization), it oscillates with frequency that depends on the size of the quantum dot and the spin-orbit coupling coefficient. And an amplitude that generally depends on the size and SOC coefficient as well. However, we also showed that for a given range of SOC coefficients, the conductance becomes size independent down to samples as small as around 2.5nm in size (r=5). This is a promising result for the realization of the QSH effect in small quantum dots. Which can be applied for example to realize billions of topological qubits on small chips. Lastly, we have demonstrated a teqnique to enhance the quantization of the spin-polarized conductance by tuning the staggered po-

tential m against the real part of the nnn-hopping t_2. This is useful as the suggested methods of increasing the spin-orbit coupling in graphene has the downside of changing the t_2 and m, which can lead to a trivial phase. We have shown that by tuning the staggered potential against t_2 we can enhance the quantization of the spin-polarized conductance, making for robust QSH effect.

A   Modeling

Graphene is a 2D material with hexagonal shaped lattice of carbon atoms, so that each carbon atom is connected to three other carbon molecules, each of them having three bonds with neighboring carbon atoms, and a bond-free p$_z$ orbital. This orbital has the free electron and therefore is of most relevance in our discussions here.

I   Tight binding

In this subsection, we will discuss the infinite 2D (periodic) model. The wavefunction of a single P$_z$ orbital will be denoted by $\phi_z(\vec{r})$.

In the hexagonal lattice, there are two atoms within the lattice, we will denote those sub-lattices with labels **A** and **B**. Due to the translational symmetry and bloch theorem, the wavefunction of the many-body system of non-interacting electrons will be given by

$$\Psi_{\vec{k}}^{\mathbf{A}}(\vec{r}) = \sum_{R_{\mathbf{A}}} e^{i\vec{R}_{\mathbf{A}}\cdot\vec{k}} \phi_z(\vec{r} - \vec{R}_{\mathbf{A}}) \tag{22}$$

Similarly with **B** sublattice (one can check that it satisfies the Bloch theorem). The general solution will be given by a linear combination of states from the two

$$\Psi_{\vec{k}} = A_{\vec{k}}\Psi_{\vec{k}}^{\mathbf{A}} + B_{\vec{k}}\Psi_{\vec{k}}^{\mathbf{B}} \tag{23}$$

The general 1 particle Hamiltonian of the system is

$$H = \frac{1}{2m}\hat{p}^2 + \sum_{\vec{R_{\mathbf{A}}}} V(\vec{r} - \vec{R_{\mathbf{A}}}) + \sum_{\vec{R_{\mathbf{B}}}} V(\vec{r} - \vec{R_{\mathbf{B}}}) \tag{24}$$

we set the onsite energy to 0

$$H|\phi_z\rangle = \frac{1}{2m}\hat{p}^2|\phi_z\rangle + V(\vec{r})|\phi_z\rangle = 0|\phi_z\rangle \tag{25}$$

In the hexagonal lattice basis, the Hamiltonian of the system is given by

$$H(\vec{k}) = \begin{pmatrix} H_{\mathbf{AA}}(\vec{k}) & H_{\mathbf{AB}}(\vec{k}) \\ H_{\mathbf{BA}}(\vec{k}) & H_{\mathbf{BB}}(\vec{k}) \end{pmatrix} \tag{26}$$

In the nearest neighbor interactions approximation

$$H_{\mathbf{AA}}(\vec{k}) = \langle\Psi_{\vec{k}}^{\mathbf{A}}|H|\Psi_{\vec{k}}^{\mathbf{A}}\rangle \tag{27}$$

$$H_{\mathbf{AA}}(\vec{k}) = \sum_{\vec{R_{\mathbf{A}}}}\sum_{\vec{R_{\mathbf{A}}}'}\sum_{\vec{R_{\mathbf{B}}}} \int \phi_z(\vec{r} - \vec{R_{\mathbf{A}}})\phi_z(\vec{r} - \vec{R_{\mathbf{A}}}')V(\vec{r} - \vec{R_{\mathbf{B}}}) \tag{28}$$

$$H_{\mathbf{AA}}(\vec{k}) = \sum_{<\vec{R_{\mathbf{A}}},\vec{R_{\mathbf{B}}}>}\sum_{<\vec{R_{\mathbf{A}}}',\vec{R_{\mathbf{B}}}>} \int \phi_z(\vec{r} - \vec{R_{\mathbf{A}}})\phi_z(\vec{r} - \vec{R_{\mathbf{A}}}')V(\vec{r} - \vec{R_{\mathbf{B}}}) \tag{29}$$

$$H_{\mathbf{AA}}(\vec{k}) = \sum_{<\vec{R_{\mathbf{A}}},\vec{R_{\mathbf{B}}}>} \int \phi_z(\vec{r} - \vec{R_{\mathbf{A}}})^2 V(\vec{r} - \vec{R_{\mathbf{B}}}) \tag{30}$$

$$H_{\mathbf{AA}}(\vec{k}) = 0 \quad V \text{ is localized} \tag{31}$$

similarly $H_{\mathbf{BB}}(\vec{k}) = 0$ in the nearest neighbor approximation

$$H_{\mathbf{AB}}(\vec{k}) = \langle \Psi^{\mathbf{A}}_{\vec{k}} | H | \Psi^{\mathbf{B}}_{\vec{k}} \rangle \tag{32}$$

$$H_{\mathbf{AB}}(\vec{k}) = \sum_{\vec{R_A}} \sum_{\vec{R_B}} \sum_{\vec{R_B}'} e^{i\vec{k}\cdot(\vec{R_A}-\vec{R_B})} \int \phi_z(\vec{r}-\vec{R_A})\phi_z(\vec{r}-\vec{R_B}')V(\vec{r}-\vec{R_B}) \tag{33}$$

$$H_{\mathbf{AB}}(\vec{k}) = \sum_{\vec{R_A}} \sum_{\vec{R_B}} e^{i\vec{k}\cdot(\vec{R_A}-\vec{R_B})} \int \phi_z(\vec{r}-\vec{R_A})\phi_z(\vec{r}-\vec{R_B})V(\vec{r}-\vec{R_B}) \tag{34}$$

$$H_{\mathbf{AB}}(\vec{k}) = \sum e^{i\vec{k}\cdot(\vec{R_A}-\vec{R_B})}t \tag{35}$$

$$H_{\mathbf{AB}}(\vec{k}) = \left[e^{i\vec{k}\cdot\vec{b}} + e^{i\vec{k}\cdot(\vec{a_1}-\vec{b})} + e^{i\vec{k}\cdot(\vec{a_2}-\vec{b})} \right] t \tag{36}$$

$$\tag{37}$$

where $\vec{b} = a\hat{j}$, $\vec{a}_1 = a\sqrt{3}/2\hat{i} + 3a/2\hat{j}$ and $\vec{a}_2 = -a\sqrt{3}/2\hat{i} + 3a/2\hat{j}$

$$H_{\mathbf{AB}}(\vec{k}) = f(\vec{k})t \tag{38}$$

$$f(\vec{k}) = e^{ik_x a\sqrt{3}/2 + ik_y a/2} + e^{-ik_x a\sqrt{3}/2 + ik_y a/2} + e^{-ik_y a} \tag{39}$$

$$f(\vec{k}) = 2e^{ik_y a/2} \cos k_x a\sqrt{3}/2 + e^{-ik_y a} \tag{40}$$

Similarly: $H_{\mathbf{BA}}(\vec{k}) = [H_{\mathbf{AB}}(\vec{k})]^*$. The Hamiltonian matrix (equation 26) becomes

$$H = t \begin{pmatrix} 0 & f(\vec{k}) \\ f(\vec{k})^* & 0 \end{pmatrix} \tag{41}$$

The Hamiltonian can be written in second quantization formalization as following

$$H = tf(\vec{k})a^{\dagger}_{\vec{k}}b_{\vec{k}} + tf(\vec{k})^* b^{\dagger}_{\vec{k}}a_{\vec{k}} \tag{42}$$

where $a_{\vec{k}}(b_{\vec{k}})$ is annihilation operators of A (B) sublattice electrons with momentum $\vec{k}$. Using Inverse Fourier transformation 42 can be written in real space as

$$H = -t \sum_i [a^{\dagger}_i b_i + a^{\dagger}_i b_j + a^{\dagger}_i b_k] + h.c \tag{43}$$

where the sites j, k are such that they are neighboring to site i, we can then remove the distinction between A and B sublattices and write the tight binding Hamiltonian as

$$H = -t \sum_{\langle i,j \rangle} c^{\dagger}_i c_j \tag{44}$$

We will be mostly using hamiltonian 44 unless explicitly mentioned otherwise. Notice also that hamiltonian 44 is not only restricted to periodic systems, therefore we will be using to model quantum dots as well.

Finite system

In the finite system, we do not have translational symmetry, and therefore the wavefunction will not be a Bloch wavefunction. Yet it is still possible to use the tight binding model in the real space to describe the system, therefore the Hamiltonian will be given by equation44.

Peierls substitution

In the presence of magnetic field, the hopping term (t) will acquire a Peierls phase to accommodate for the magnetic field applied to the system

$$t_{ij} \rightarrow t_{ij} \exp\left\{ \left(i\frac{e}{\hbar} \int_{\vec{r}_i}^{\vec{r}_j} \vec{A}(\vec{r}) \cdot d\vec{\ell} \right) \right\} \tag{45}$$

Next nearest neighbor hopping

In the tight binding model, we can also include the next nearest neighbor hopping (NNN) term, which is given by

$$H' = -(t_2 \pm t_{\text{SOC}}) \sum_{\langle\langle i,j \rangle\rangle} c_i^\dagger c_j + h.c \tag{46}$$

The term t_{SOC} is the spin-orbit coupling term according to the Kane-Mele model[11]. Its sign depedns on the spin of the spin of the electron considered on the site. t_2 is the real part of the NNN hopping. The SOC term is important for the QSH effect. In the case of significant nnn hopping terms, the dirac effective mass modelI.2 will no longer be valid.

staggered potential

The staggered potential is a term that breaks the sublattice symmetry, it is given by

$$H_m = \sum_i m c_i^\dagger c_i \tag{47}$$

where m is the staggered potential parameter. This term is important for the QSH effect, as it opens a bulk gap in the system. The staggered potential can be thought of as a difference in the chemical potential between the two sublattices.

Including spin

In the tight binding model, we can also include the spin degree of freedom. The Hamiltonian will then be given by

$$H = -t \sum_{\langle i,j \rangle} c_{i\sigma}^\dagger c_{j\sigma} + h.c \tag{48}$$

where $c_{i\sigma}^\dagger$ is the creation operator of an electron with spin σ on site i.

I.1 Total Hamiltonian

The most general Hamiltonian of the system will be given by

$$H = -t \sum_{\langle i,j \rangle} c_{i\sigma}^\dagger c_{j\sigma} + h.c - (t_2 + (-1)^{k(\sigma)} t_{\text{SOC}}) \sum_{\langle\langle i,j \rangle\rangle} c_{i\sigma}^\dagger c_{j\sigma} + h.c + \sum_i \left((-1)^{s(i)} m + p(i) d \right) c_{i\sigma}^\dagger c_{i\sigma}$$

(49)

where $k(\sigma)$ is the spin index, $k(\uparrow) = 0$ and $k(\downarrow) = 1$. $s(i)$ is the sublattice index, $s(i) = 0$ for sublattice A and $s(i) = 1$ for sublattice B. The Hamiltonian49 is the one we will be using in our calculations unless otherwise mentioned.

I.2 Effective mass Dirac Model

The corresponding reciprocal lattice of the hexagonal lattice is also a hexagonal lattice. The vertices of this lattice in the first quadrant are $(\vec{k} = \{[2\pi/3\sqrt{3}a \quad 2\pi/3a]^T, [4\pi/3\sqrt{3}a \quad 0]^T\})$, these are called the Dirac point, by expanding equation40 at $\vec{k}_d = [4\pi/3\sqrt{3}a \quad 0]$ point we get

$$f(\vec{k}_d + d\vec{k}) = 2e^{idk_y/2} \cos\left(2\pi/3 + a\sqrt{3}/2 dk_x\right) + e^{-idk_y}$$

(50)

$$f(\vec{k}_d + d\vec{k}) = (1 + i\frac{a}{2}dk_y)\left(\frac{3a}{2}dk_x - 1\right) + 1 - ia\, dk_y$$

(51)

$$f(\vec{k}_d + d\vec{k}) = \frac{3a}{2}dk_x - i\frac{3a}{2}dk_y$$

(52)

$$f(\vec{k}_d + d\vec{k})^* = \frac{3a}{2}dk_x + i\frac{3a}{2}dk_y$$

(53)

The Hamiltonian becomes

$$H = \frac{3}{2}a\,\vec{\sigma} \cdot d\vec{k} = v\,\vec{\sigma} \cdot \vec{p}$$

(54)

or

$$H = \frac{3}{2}a\,\vec{\sigma} \cdot d\vec{k} = -iv\,\vec{\sigma} \cdot \nabla$$

(55)

where $\vec{\sigma} = [\sigma_x \quad \sigma_y \quad \sigma_z]^T$ and $v = 3a/2\hbar$

Using another non-equivalent Dirac point $\vec{k}_d = [-4\pi/3\sqrt{3}a \quad 0]^T$ we get the following Hamiltonian

$$H = v\vec{\sigma} \cdot \vec{p}$$

(56)

Combining both55 and56 using the following a basis of $[\psi_K^A \quad \psi_K^B \quad \psi_{K'}^B \quad \psi_{K'}^A]^T$, the Dirac Hamiltonian of the graphene system is given by

$$H = v\tau_0 \otimes \vec{\sigma} \cdot \vec{p}$$

(57)

IV

Equation 57 establishes that fermions in graphene behave similarly to massless Dirac fermions with linear rather than quadratic energy dispersion near Dirac points.

B Local density and local current density

The local density is given simply by $\langle\psi|i\rangle\langle i|\psi\rangle$, where $|i\rangle$ is the ith site. And $|\psi\rangle$ is the wavefunction of the system. The spin polarized local density will be given by $\langle\psi|i\rangle\langle i|\sigma_3|\psi\rangle$. Where σ_3 is the z Pauli matrix that corresponds to the spin degree of freedom. The total current density on the other hand is given by (we set $\hbar = 1$)

$$J_{i\to j} = i\left(\langle j|\hat{H}_{ij}^\dagger|i\rangle - \langle i|\hat{H}_{ij}|j\rangle\right) \tag{58}$$

Where $\hat{H}_{ij}$ is the hopping matrix between sites i and j. The spin polarized current density is given by

$$J_{i\to j}^\sigma = i\left(\langle j|\sigma_3\hat{H}_{ij}^\dagger|i\rangle - \langle i|\hat{H}_{ij}\sigma_3|j\rangle\right) \tag{59}$$

The calculations were performed using the Kwant package[8] in Python.

C landauer-Büttiker formula

The Landauer-Büttiker formula[2] is a way to calculate the conductance of a quantum system in the presence of leads. It is based on the idea that the conductance can be calculated from the transmission coefficients of the system. One treats the system as a scattering problem, where the leads are treated as reservoirs that can exchange particles with the system. So given a system with hamiltonian H and two leads. Assuming the incoming electrons are plane waves $e^{-ikn} + re^{ikn}$ and the outgoing electrons are te^{ikn}. The boundary conditions at the leads are continuity conditions. Therefore, the hamiltonian can be written as

$$\mathcal{H} = \begin{pmatrix} H_l & V_l & 0 \\ V_l^\dagger & H & V_r^\dagger \\ 0 & V_r & H_r \end{pmatrix} \tag{60}$$

As for our case of single chain leads, H_l and H_r are 1x1 onsite matrices on additional sites, and V is a 1xN matrix, given by the hopping between the leads and the nearest site in the system, zero otherwise. The scattering problem is then written as

$$\begin{pmatrix} 0 & V_l & 0 \\ V_l^\dagger & H & V_r^\dagger \\ 0 & V_r & 0 \end{pmatrix} \begin{pmatrix} \psi_l \\ \psi \\ \psi_r \end{pmatrix} = E \begin{pmatrix} \psi_l \\ \psi \\ \psi_r \end{pmatrix} \tag{61}$$

Where $\langle n|\psi_l\rangle = Ae^{ikn} + Be^{-ikn}$ and $\langle n|\psi_r\rangle = A'e^{ikn} + A'e^{-ikn}$. By substituting the wavefunctions into the above equation, one gets the generalized eigenvalue problem

$$(H' - E\mathbb{I}) = C \tag{62}$$

V

Where H' is the Hamiltonian of the system with additional onsite potential on lead contacts given by $H'_{ij} = H_{ij} - (\delta_{1i}\delta_{1j} + \delta_{Nj}Nj)t$. And C is the boundary condition matrix. Here we did not directly solve the eigenvalue problem, but rather used the Kwant package[8] to solve the scattering problem. Which is more optimized for large systems.

D Edge states in Large Graphene quantum dot

Here we reproduced results from[20]. We solve the tight-binding model for a realistic sized graphene deformed circular quantum dot with the following Hamiltonian1

$$H = -t \sum_{\langle i,j \rangle} c_i^\dagger c_j + \text{h.c} - t' \sum_{\langle\langle i,j \rangle\rangle} c_i^\dagger c_j + \text{h.c} + U_0 \sum_{\text{edge}} c_i^\dagger c_i \tag{63}$$

This Hamiltonian was used in[20]. Due to the large size of the system (more than 190000 sites) the Hamiltonian was solved using Matlab. The density of states was confirmed to match the results in the paperD.1,D.2 andD.3
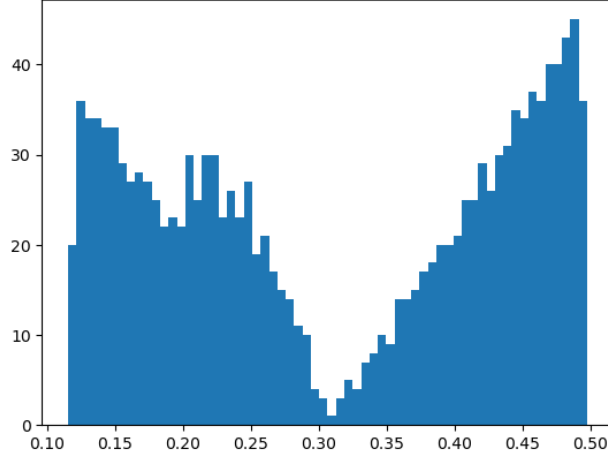
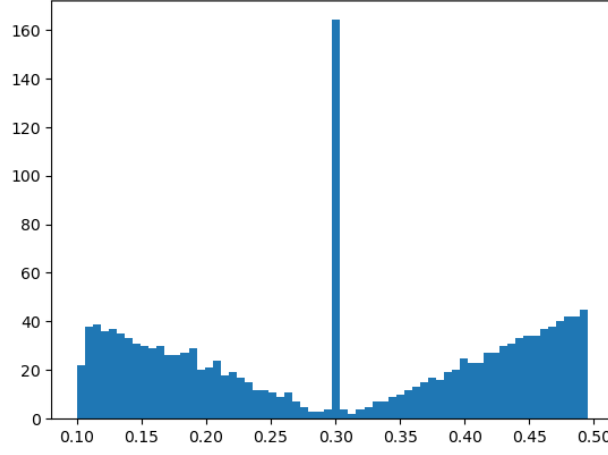Figure D.1: DOS (Number of states vs. Energy) for $U_0 = 0, t' = 0.1t$

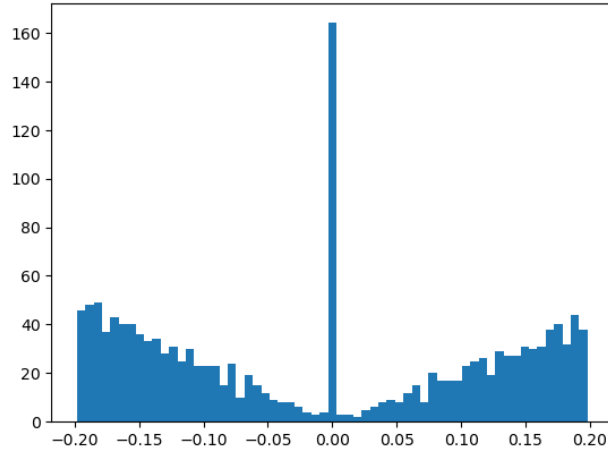Figure D.2: DOS (Number of states vs. Energy) for $U_0 = 0.1t, t' = 0.1t$

Figure D.3: DOS (Number of states vs. Energy) for $U_0 = 0, t' = 0$

E Solutions and Codes

The codes used to solve the problems in this work are available on GitHub[12]. The codes are written in Python and use the Kwant package[8] for solving the tight binding model. Some eigenvalue problems were solved in matlab for better performance (such as the results in D.1,D.2 and D.3).

References

[1] AR Akhmerov and CWJ Beenakker. "Boundary conditions for Dirac fermions on a terminated honeycomb lattice". In: *Physical Review B—Condensed Matter and Materials Physics* 77.8 (2008), p. 085423.

[2] Philip B Allen. "Electron transport". In: *Contemporary Concepts of Condensed Matter Science* 2 (2006), pp. 165–218.

[3] Mitchell Bacon, Siobhan J Bradley, and Thomas Nann. "Graphene quantum dots". In: *Particle & Particle Systems Characterization* 31.4 (2014), pp. 415–428.

[4] Paolo Bordone, Laura Bellentani, and Andrea Bertoni. "Quantum computing with quantum-Hall edge state interferometry". In: *Semiconductor Science and Technology* 34.10 (2019), p. 103001.

[5] Luis Brey and HA Fertig. "Electronic states of graphene nanoribbons studied with the Dirac equation". In: *Physical Review B—Condensed Matter and Materials Physics* 73.23 (2006), p. 235411.

[6] Antonio H Castro Neto et al. "The electronic properties of graphene". In: *Reviews of modern physics* 81.1 (2009), pp. 109–162.

[7] Motohiko Ezawa. "Metallic graphene nanodisks: Electronic and magnetic properties". In: *Physical Review B—Condensed Matter and Materials Physics* 76.24 (2007), p. 245415.

[8] Christoph W Groth et al. "Kwant: a software package for quantum transport". In: *New Journal of Physics* 16.6 (2014), p. 063065.

[9] VP Gusynin and SG Sharapov. "Unconventional integer quantum Hall effect in graphene". In: *Physical review letters* 95.14 (2005), p. 146801.

[10] Huaqing Huang and Feng Liu. "Theory of spin Bott index for quantum spin Hall states in nonperiodic systems". In: *Physical Review B* 98.12 (2018), p. 125130.

[11] Charles L Kane and Eugene J Mele. "Quantum spin Hall effect in graphene". In: *Physical review letters* 95.22 (2005), p. 226801.

[12] Hasan. Khaled. *Graphene Quantum dots.* https://github.com/khaledoqab/Graphene_QD. 2025.

[13] Edward McCann and Vladimir I Fal'ko. "Symmetry of boundary conditions of the Dirac equation for electrons in carbonnanotubes". In: *Journal of Physics: Condensed Matter* 16.13 (2004), p. 2371.

[14] Satoshi Morita and Hidetoshi Nishimori. "Mathematical foundation of quantum annealing". In: *Journal of Mathematical Physics* 49.12 (2008).

[15] U Sivan, Yoseph Imry, and C Hartzstein. "Aharonov-Bohm and quantum Hall effects in singly connected quantum dots". In: *Physical Review B* 39.2 (1989), p. 1242.

[16] U. Sivan, Y. Imry, and C. Hartzstein. "Aharonov-Bohm and quantum Hall effects in singly connected quantum dots". In: *Phys. Rev. B* 39 (2 Jan. 1989), pp. 1242–1250. DOI: 10.1103/PhysRevB.39.1242. URL: https://link.aps.org/doi/10.1103/PhysRevB.39.1242.

[17] Daniele Toniolo. "On the Bott index of unitary matrices on a finite torus". In: *Letters in Mathematical Physics* 112.6 (2022), p. 126.

[18] Conan Weeks et al. "Engineering a robust quantum spin Hall state in graphene via adatom deposition". In: *Physical Review X* 1.2 (2011), p. 021001.

[19] Alexander Weiße et al. "The kernel polynomial method". In: *Reviews of modern physics* 78.1 (2006), pp. 275–306.

[20] M Wimmer, AR Akhmerov, and F Guinea. "Robustness of edge states in graphene quantum dots". In: *Physical Review B—Condensed Matter and Materials Physics* 82.4 (2010), p. 045409.

[21] Di Xiao, Ming-Che Chang, and Qian Niu. "Berry phase effects on electronic properties". In: *Reviews of modern physics* 82.3 (2010), pp. 1959–2007.